Available online at www.sciencedirect.com
SCIENCE DIRECT®
Ultrasonics 42 (2004) 519–526
Ultrasonics
www.elsevier.com/locate/ultras

Ultrasonic characterization of Cu–Al–Ni single crystals lattice stability in the vicinity of the phase transition

Michal Landa [a,*], Václav Novák [b], Petr Sedlák [a], Petr Šittner [b]

[a] Institute of Thermomechanics, Academy of Sciences, Dolejškova 5, 182 00 Praha 8, Czech Republic
[b] Institute of Physics, Academy of Sciences, Na Slovance 2, 182 21 Praha 8, Czech Republic

Abstract

Measurements of elastic constants of the austenite phase when approaching the phase transformation either upon cooling or stressing is of the crucial interest for the shape memory alloy field. Acoustic properties (wave velocity and also attenuation changes) of the Cu–Al–Ni single crystal were investigated in situ during stress-induced martensitic transformation at constant (room) temperature. The parent austenite cubic lattice of the Cu–Al–Ni exhibits very high elastic anisotropy (anisotropy factor A∼12). The measurements were made using nine combinations of (i) applied uniaxial compression in a given crystal direction, (ii) the wave propagation and (iii) polarization vectors. The chosen configurations are sufficient for evaluation of all independent third order elastic constants (TOEC). The longitudinal modes were also measured by the immersion technique, using the transducer pair in a water tank installed on the testing machine. The device works as "a ultrasonic extensometer" measuring a transverse strain of the specimen. The dependencies of both natural and initial wave velocities on the applied stress may be evaluated. Three elastic constants of the stress-induced martensite were determined. The elastic properties were found to vary with the increasing stress above the Ms transformation temperature, which is interpreted as a precursor for the martensitic transformation. The onset of the transformation was additionally identified from the acoustic emission measurement.

Keywords: Crystal acoustics; Phase transitions; Acoustoelasticity; Digital-pulse-echo methods

1. Introduction

The unique properties of shape memory alloys (SMAs) derive from thermo-elastic martensitic transformation (MT) in solid state driven by the external stress and temperature. Typically, the SMAs are intermetallic ordered alloys (Cu–Al–Ni, Cu–Zn–Al, Ni–Ti, Ni–Mn–Ga, etc.), often strongly elastically anisotropic. When the stress-induced MT proceeds in the SMA single crystal, it becomes a sort of metastable two phase composite consisting of plate-like particles of martensite within the parent austenite phase. The phases are separated by highly mobile phase interfaces and have different elastic constants. Knowledge of the elastic constants (second order elastic constant—SOEC) of both phases in SMAs is essential to describe reliably their mechanical behaviors.

The third order elastic constants (TOEC) play a primary role in understanding of the anharmonic and nonlinear properties of solids [1]. Therefore, investigation of the TOECs is a key to the understanding of the lattice stability of SMAs [2]. In Ref. [2], a complete set of TOECs of the cubic austenite phase of Cu-based SMAs single crystals around and far above the transformation temperature was measured. The TOECs are determined from the initial slope of the stress dependence of the velocity of the propagation of ultrasonic wave through the crystal. The TOECs were used to determine the acoustic model Grüneisen parameters.

2. Specimen

A single crystal of Cu-14.3% Al-4.1% Ni (wt.%) alloy was prepared by the Bridgman method. The crystal structure at room temperature is bcc (cubic austenite β-phase), because the transition temperature ($M_s \sim 193$ K) to the martensite phase is much lower. A cube specimen

* Corresponding author. Fax: +4202-858-4695.
E-mail address: ml@it.cas.cz (M. Landa).

0041-624X/$ - see front matter © 2004 Elsevier B.V. All rights reserved.
doi:10.1016/j.ultras.2004.01.029

(of about $10\times10\times10$ mm^3) was cut with faces perpendicular to the [1 1 0], [$\bar{1}$ 1 0] and [0 0 1] crystallographic axes. By temperature decrease below M_s or by applied compression stress, the austenite phase can be transformed into the martensite of orthorhombic 2H structure (in Ramsdell notation). The phase change is accompanied by a shape change. Upon subsequent heating or unloading, the parent austenite phase and shape are restored.

3. SOECs measurement

The standard pulse-echo method [3] was used for the measurement of the velocity of longitudinal (L, qL) and transversal waves (T and qT) propagating in the principal axes of the stress-free single crystal at RT (Table 1). The mass density ρ_0 of the specimen was evaluated by the Archimedes technique. The relative standard deviation of the velocities and the mass density was estimated as 0.16%, 0.3%, respectively. The evaluated SOECs C_{11}, C_{12}, C_{44} are given in Table 2. The resulting C_{12} is an average value evaluated directly from the qL and qT velocities. The other qL and qT velocities in the direction [1 1 1] are calculated and added in Table 1. The very strong anisotropy is demonstrated by the section of the phase velocity diagram in a principal plane (Fig. 1). The larger deviations of shear velocities measurements (Table 2) can be explained by increasing demands on the precision of the sample cut and directional accuracy of the ultrasonic measurement, the alignment of shear waves polarization, in particular. The measured elastic properties of β-phase of Cu–Al–Ni are in good agreement with the published data [2].

4. TOECs measurement

The acoustoelastic properties of a cubic crystal are given by the three independent SOECs (above) and by six TOECs: C_{111}, C_{112}, C_{123}, C_{144}, C_{166} and C_{456}, [4]. As derived in [5], the TOECs may be evaluated from the known SOECs and nine directional configurations (Table 2 and Fig. 2) of wave velocity measurements in the single crystal cut with faces normal to the [1 1 0], [$\bar{1}$ 1 0] and [0 0 1] directions, during uniaxial compression. The martensitic transformation starts, as evidenced by mechanical curves at compressive stresses 400 MPa (modes 1–3) and 800 MPa (modes 4–9). The difference is due to the orientation dependence of transformation stress of the cubic to orthorhombic transformation. The redundant number of measurements has been utilized to improve the TOECs determination.

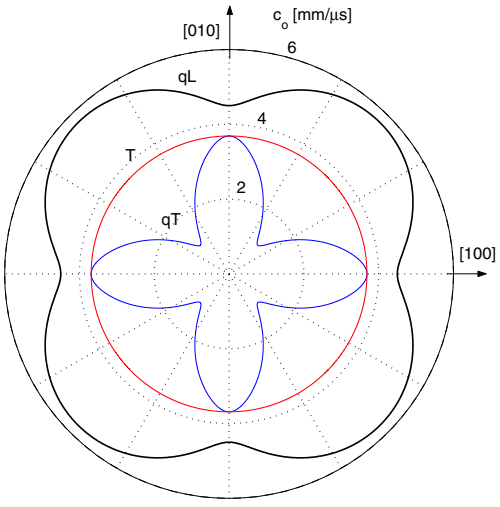

Fig. 1. The (0 0 1) plane cut of the qL, T and qT phase velocity surfaces.

Using quartz X and Y-cut (10 MHz both), the longitudinal and transversal waves were generated in the direction N perpendicular to the compression axis M. The polarization direction is then marked as U (Fig. 2). The 50 MHz pulse/receiver system DPR50+ (JSR Ultrasonics) and the oscilloscope Waverunner 2 LT264M (LeCroy) were utilized for echo measurement

Table 1
Wave velocity measurement in the stress-free single crystal of the Cu–Al–Ni alloy at RT

Directions	Velocity $c_0[N][U]$					
	Measured				Calculated	
[N]:	[0 0 1]	[0 0 1]	[1 1 0]	[1 1 0]	[1 1 1]	[1 1 1]
[U]:	[0 0 1]	(0 0 1)	[1 1 0]	[$\bar{1}$ 1 0]	[1 1 1]	(1 1 1)
c_0 (mm/μs)	4.499	3.687	5.719	1.060	6.071	2.300
std (c_0) (mm/μs)	–	±0.006	±0.001	±0.004	–	–

Table 2
SOECs and related elastic constants of Cu–Al–Ni austenite phase

ρ_0 (g/cm^3)	C_{11} (GPa)	C_{12} (GPa)	C_{44} (GPa)	A [1]	C_L (GPa)	C' (GPa)
7.055	142.80	126.84 ± 0.15	95.90 ± 0.30	12.02	230.73	7.98

$A = 2C_{44}/(C_{11} - C_{12})$, $C' = (C_{11} - C_{12})/2$, $C_L = (C_{11} + C_{12})/2 + C_{44}$.

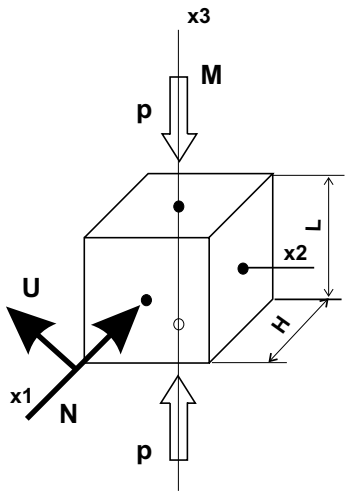

Fig. 2. Loading of the cubic specimen and ultrasonic wave propagation.

in each loading step. The acquired signals were averaged and recorded with the equivalent sampling frequency 10 GS/s. The actual time of flight (TOF) was obtained adopting cross-correlation technique during digital signal postprocessing. The wave velocities v_0 were related to the natural (stress-free, undeformed) state L_0.

The experiments were performed on the electromechanical test machine TiraTest 2300 (100 kN). The loading of the specimen was realized over the spherical joint to suppress additional shear stress effect (Fig. 4). All measurements were carried out at temperature $T = 297 \pm 1$ K. Temperature differences among the measured cycles were not greater than 2 K and a temperature variation during one cycle did not exceed 1 K.

The measured wave velocity changes with respect to the stress-free natural state are shown in Fig. 3, where the wave modes L and qL, T and qT modes were plotted, separately. Variations of actual wave velocity v_0 from the velocity value c_0 in the stress-free specimen were normalized by c_0. The mode #(8) was measured only for compression stress up to 18 MPa. Due to the additional anisotropy caused by the applied uniaxial stress, the energy flux considerably changes direction from the wave vector and the echo rapidly decays with the increasing compression stress.

The slopes in the vicinity of $p = 0^+$ were obtained by the linear regression of the initial part of the dependencies. Adopting the least-square method over all nine configurations (Table 3), the TOECs were determined from the measured values of $\{d(\rho_0 v_0^2)/dp\}_{p=0}$. The slope deviations were taken into account in the calculation as weight factors. The wave velocity measured in mode #(5) shows an extremely low sensitivity to applied stress but large scatter. Hence, the corresponding value was taken as a free parameter and adjusted to the value given in the rightmost column during the fitting procedure. In such a way determined TOECs are written in Table 4 with the error ranges (correlation $r = 0.9998$). The TOECs are very sensitive to the SOECs deviations, mainly to the C_{12}. The TOECs values differ up to about 50% from the values measured on a similar alloy [2] ($A = 13.1$) at temperature $T = 293$ K. Nevertheless, the measured values of TOECs fulfil the conditions

$$C_{ijk} < 0, \quad \text{and } C_{111} < C_{112} < C_{123}, \tag{1}$$

arising from the atomic binding force relation [4].

The qT modes #(8) and #(2) are the most sensitive ones to the applied stress. This can be ascribed to the intrinsic shear instability associated with the martensitic transformation, the critical condition of which is being approached upon stressing. The configuration #(4) is the next most sensitive one. The stress dependence of the longitudinal velocity in this mode shows a noticeable hysteresis. The measurement was several times repeated to eliminate an experimental error, but the hysteresis was always evident. The configurations #(6), #(5) and #(9) show a similar though less pronounced hysteresis.

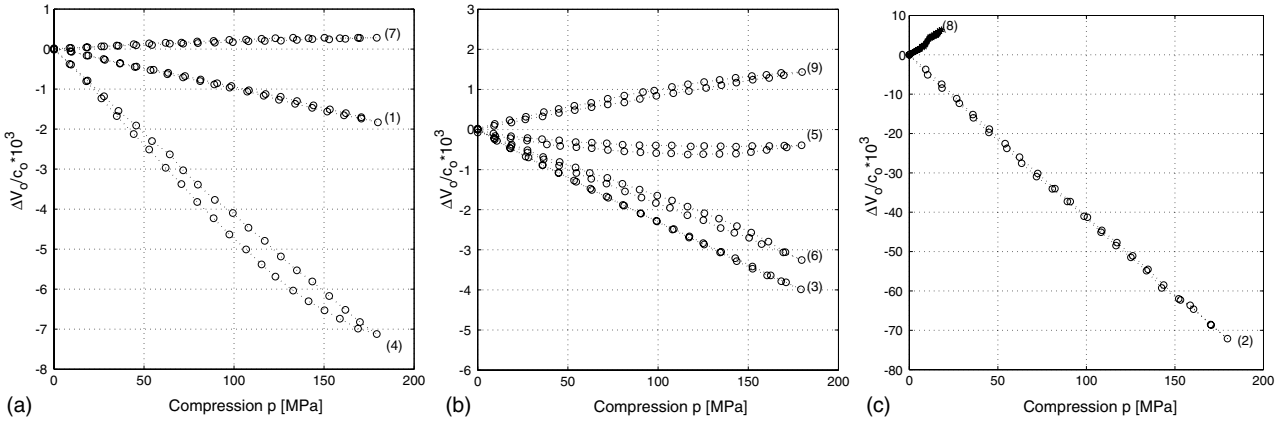

Fig. 3. Acoustoelastic property of the Cu–Al–Ni single crystal(austenite) represented by natural velocity changes $\Delta v_0/c_0$. Configuration types: (a) L and qL, (b) T and (c) qT modes.

Table 3
Measured velocity slopes $\{d(\rho_0 v_0^2)/dp\}_{p=0}$ and fitted ones by TOEC evaluation procedure

Test no.	Wave mode	Directions			$\{d(\rho_0 v_0^2)/dp\}_{p=0}$	
#	$(\rho_0 v_0^2)_{p=0}$	M	N	U	Input	Fitted
(1)	C_L	[0 0 1]	[1 1 0]	[1 $\bar{1}$ 0]	-4.41 ± 0.19	−4.40
(2)	C'	[0 0 1]	[1 1 0]	[$\bar{1}$ 1 0]	-7.01 ± 0.11	−7.04
(3)	C_{44}	[0 0 1]	[1 1 0]	[0 0 1]	-4.75 ± 0.12	−4.74
(4)	C_{11}	[$\bar{1}$ 1 0]	[0 0 1]	[0 0 1]	-13.30 ± 0.54	−13.41
(5)	C_{44}	[$\bar{1}$ 1 0]	[0 0 1]	[$\bar{1}$ 1 0]	x	1.01
(6)	C_{44}	[$\bar{1}$ 1 0]	[0 0 1]	[1 1 0]	-3.71 ± 0.11	−3.79
(7)	C_L	[$\bar{1}$ 1 0]	[1 1 0]	[1 1 0]	1.06 ± 0.11	1.06
(8)	C'	[$\bar{1}$ 1 0]	[1 1 0]	[$\bar{1}$ 1 0]	4.29 ± 0.13	4.20
(9)	C_{44}	[$\bar{1}$ 1 0]	[1 1 0]	[0 0 1]	1.48 ± 0.19	1.72

Table 4
TOECs of Cu–Al–Ni austenite phase

TOECs (TPa)	
C_{111}	-1.65 ± 0.17
C_{112}	-0.62 ± 0.13
C_{123}	-0.48 ± 0.08
C_{144}	-0.60 ± 0.08
C_{166}	-0.69 ± 0.01
C_{456}	-0.56 ± 0.06

The hysteresis in elastic properties is not generally expected in mechanical cycle in elastic range. One has to be, however, careful, since the compression stress (200 MPa) applied in the present work was much higher compared to the level commonly used in TOECs studies [2]. There is a danger that the MT already started in the mechanical cycles. In fact, the hysteresis can be considered as a sign of the martensitic transformation. So we would like to be sure that the MT did not start at stresses below 200 MPa. Hence, the single crystal loaded/unloaded through the transformation range up to the final martensite phase while the ultrasonic measurements were carried out using the measurement configuration #(1).

5. Ultrasonic measurement during MT

The usage of the ultrasonic immersion system (Fig. 4) in the acoustoelastic measurement was motivated by the fact that

- it is noncontact—sample surface deformation has an influence to acoustic coupling of the direct contact transducers, which is eliminated by the suggested technique,
- simultaneously measurement of the crystal thickness and TOF, which enable to determine the transversal strain and the instantaneous velocity [6].

Two immersion transducers LS 25-10 (10 MHz/0.25″, Ultran) and two channels Ultrasound card SFT4003B

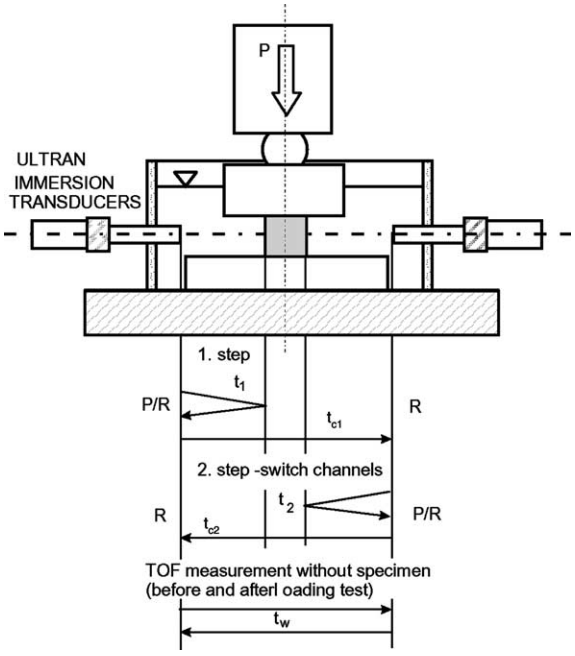

Fig. 4. Experimental arrangement of the immersion technique.

(Sofratest) were used for this experiment. The ultrasonic signals were processed by the digital storage oscilloscope and recorded via GPIB. The TOFs were obtained by cross-correlation, threshold level, zero over crossing and peak detection methods. This multi-detection approach makes the TOF evaluation more accurate. The differences among the results of the various detections indicate an influence of signal dispersion expected mainly during the MT. The peak amplitude of transmitted signals correlates well with the RMS value of the echo and it is used for attenuation analysis.

The TOF without the specimen (t_w in Fig. 4) was measured before and after each loading cycle. The ultrasonic measurement during loading of the specimen was carried out in two steps at each strain increment: one channel of the SFT card is a pulse emitter/receiver and second channel is a receiver. The first channel emits the pulse and also receives echo from the specimen with

the delay t_1, and the second channel receives the transmitted signal (t_{c1}) through the specimen. Before the second step of the ultrasound measurement, the transducers mutually swop by means of the hf-signal switch unit, designed for this purpose. The other echo, delayed about t_2 and the transmitted pulse in the time t_{c2} are detected from the opposite direction. Using two time differences

$$\begin{aligned} &\Delta t_{wm} = t_w - (t_1 + t_2)/2, \\ &\Delta t_{wc} = t_w - t_c, \quad \text{where } t_c = (t_{c1} + t_{c2})/2, \end{aligned} \tag{2}$$

we can express the instantaneous distance H and velocity v with respect to the deformed state

$$H = c_w \Delta t_{wm}, \quad \text{and} \quad v = H/(t_{wm} - t_{wc}). \tag{3}$$

The c_w is a wave speed in water (corrected to measured temperature).

The test in mode #(1) is realized by loading the crystal in the [0 0 1] direction using longitudinal wave measurement along $[\bar{1}\,1\,0]$ crystal direction. The evolution of the measured natural and instantaneous wave velocities during the test are shown in Fig. 5a and b, respectively. Three parts corresponding to the different physical processes (elastic deformation of austenite, stress-induced transformation, elastic deformation of martensite) can be clearly recognized. Regardless of what is measured during the transformation, there is a significant difference between the wave speeds measured in the austenite and martensite states. This reflects the change of the elastic properties of the crystal in the $[\bar{1}\,1\,0]_A$ direction accompanying the stress-induced phase change (Table 5).

Additionally, the transversal strain $\varepsilon_1 = \Delta H/H_0$ (Fig. 5c) was evaluated from the ultrasonic measurement of the specimen thickness evolving during the loading cycle. These data were used to evaluate the compliance components of the austenite and also the martensite phase, $S_{1'3'}(A)$ and $S_{1'3'}(M)$, respectively. The obtained values are given in Table 5 together with the measured elastic constants $C_{1'1'}$ and Young moduli $E_{3'3'}(A)$ and $E_{3'3'}(M)$ obtained from the mechanical test (Fig. 5c). The errors were estimated from the linear regression of the relevant parts at the beginning and the end of the test. The austenite values given in parenthesis are the elastic quantities in the coordinates $\{x_{1'}, x_{2'}, x_{3'}\}^T \equiv [1\,1\,0][\bar{1}\,1\,0][0\,0\,1]$, transforming from $[1\,0\,0][0\,1\,0][0\,0\,1]$

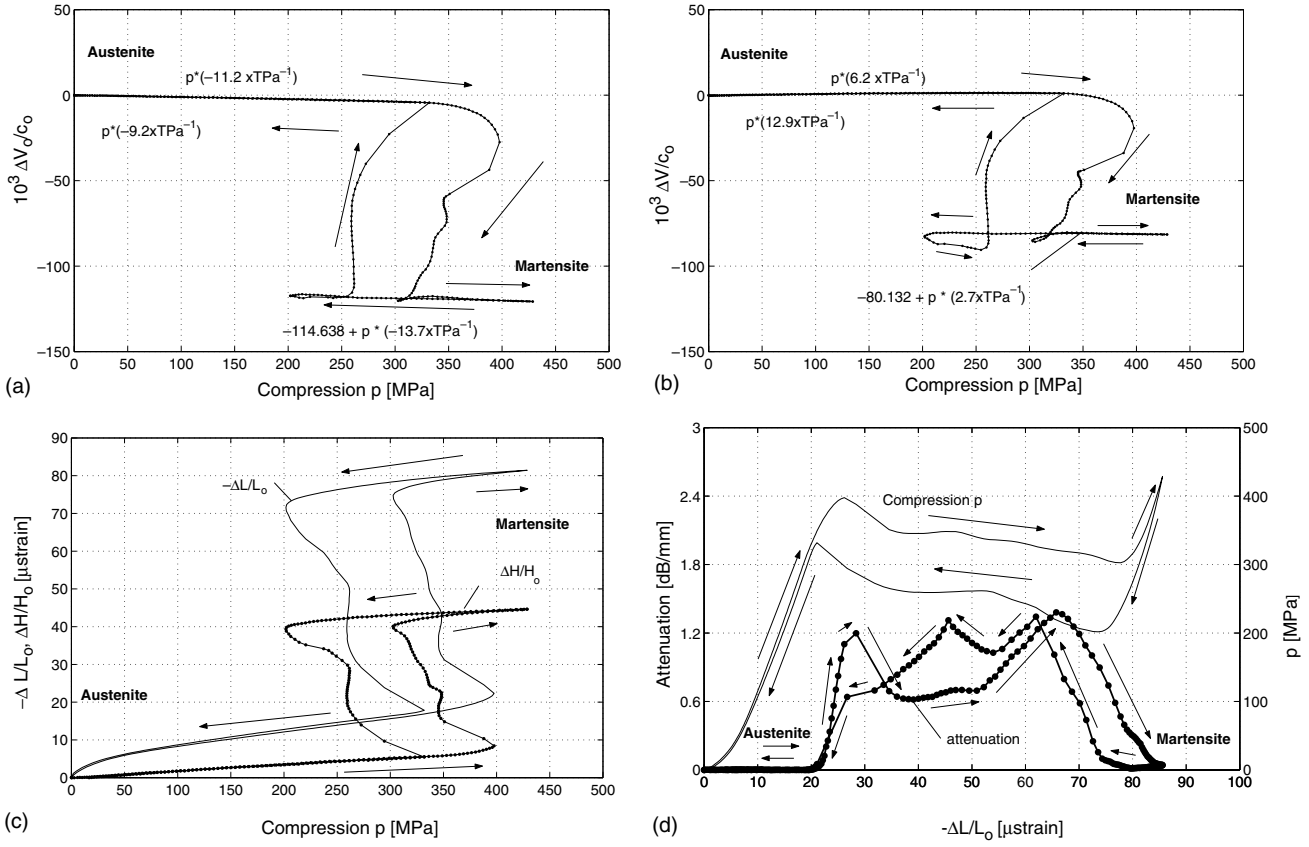

Fig. 5. Relative changes in velocity with respect to (a) natural state ($\Delta v_0/c_0$), and (b) deformed state ($\Delta v/c_0$) during the martensitic transformation of the test mode #(1); (c) ultrasonic measurement of transversal strain $\Delta H/H_0$ versus applied compression and the strain–stress relation ($-\Delta L/L_0$ versus compression p), evaluated from the measurement by displacement transducers in the compression axis; (d) The amplitude attenuation of the longitudinal wave transmitting through the specimen during the test.

Table 5
Elastic properties of austenite and martensite phase of Cu–Al–Ni evaluated from the test #(1) performed in immersion

Structure	Elastic constants in ([1 1 0][$\bar{1}$ 1 0][0 0 1]) austenite coordinates		
	$C_L \equiv C_{1'1'}$ (GPa)	$S_{1'3'}$ (1/TPa)	$E_{3'3'}$ (GPa)
Austenite	(230.73)	(−20.00)	(23.47)
Before MT	231.5 ± 0.1	−17.43 ± 0.10	25.10 ± 0.22
After MT	231.4 ± 0.1	−19.23 ± 0.12	23.04 ± 0.16
Martensite	195.5 ± 0.1	−13.08 ± 0.30	36.71 ± 0.81

calculated using the austenite elastic constants C_{ij} from Table 2.

The longitudinal velocity dramatically changes (Fig. 5a and b) during the transition between the austenite and martensite states. Since the lamellar microstructure evolves in this stage, the wave propagation is apparently affected and cannot be meaningfully interpreted.

The attenuation of the transmitted longitudinal wave was determined as a decay of the relative peak amplitude divided by the instantaneous length H of wave path. It evolution during the mechanical cycle is presented in dependence on the axial strain $\varepsilon_3 = \Delta L/L_0$ in Fig. 5d. The attenuation increases due to the material dispersion of the heterogeneous media in the range of strains 20–80 microstrain and remains practically zero outside this interval where austenite or martensite single crystals exist. There are two interesting features to point out. Firstly, the attenuation starts increase earlier (330 MPa) before the peak of the stress–strain curve evidencing the start of the macroscopic transformation process is reached. Secondly, the forward and reverse branches in the 20–80 microstrain range are significantly different. This suggest that the microstructure evolution during the forward and reverse cubic to orthorhombic transformation in Cu-based alloy single crystals are different as reported and discussed earlier e.g. for Cu–Al–Zn–Mn single crystal [7].

The martensitic transformations in SMAs are accompanied by intensive acoustic emission (AE), which can be beneficially utilized for detection and kinetic characterization of the transformation processes [8]. The AE was monitored during compression test in the next experiment. The AE activity is plotted in logarithmic scale in dependence of the strain ε_3 together with the loading curve in Fig. 6a and b (top). The start of the $A \rightarrow M$ (the finish of the $A \leftarrow M$) transformations are clearly identified as a departure (arrival) of the cumulative AE count rate from the zero value.

The relative changes of the wave velocity $\Delta V/c_0$, transversal strain ε_1 and attenuation are compared with compression stress, p and AE activity in Fig. 6a and b. The overall stress–strain curve is in Fig. 5d. Each of the five different quantities can be used to detect the start of the transformation process. The evaluated threshold

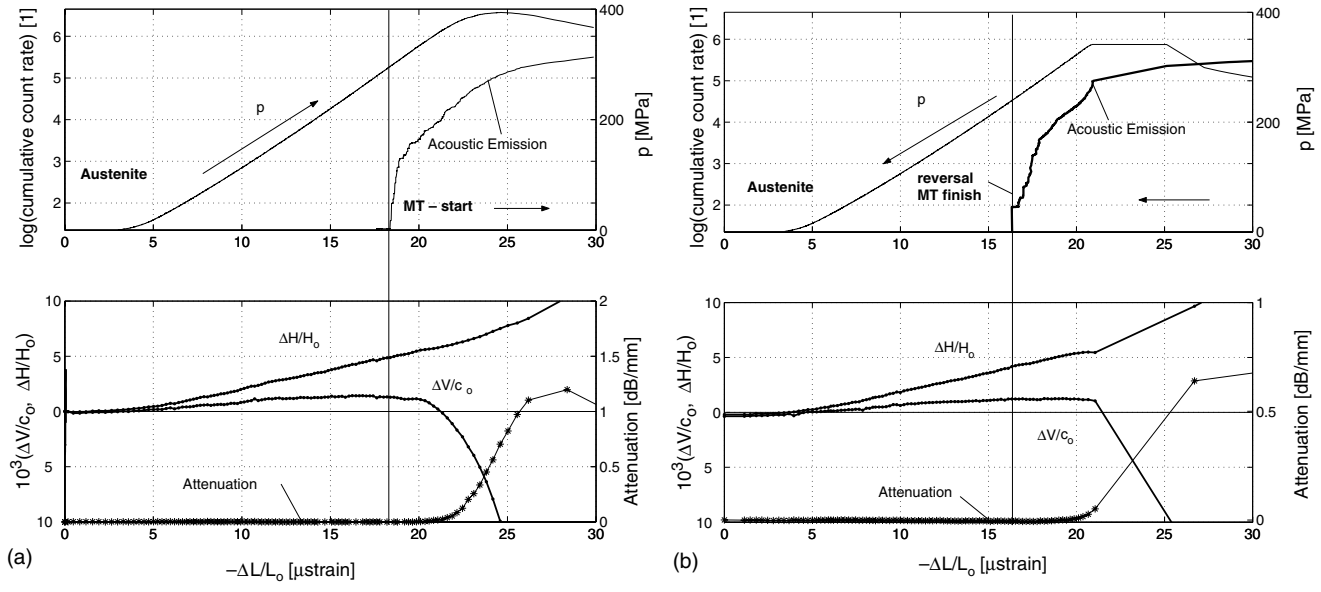

Fig. 6. Comparison of the relative changes in the velocities $\Delta v/c_0$ and the transversal strain $\Delta H/H_0$ obtained by ultrasound with the acoustic emission activity detecting during a next loading cycle. (a) MT start and (b) reversal MT finish were determined by increasing of AE counts forward and backward cumulative sum, respectively.

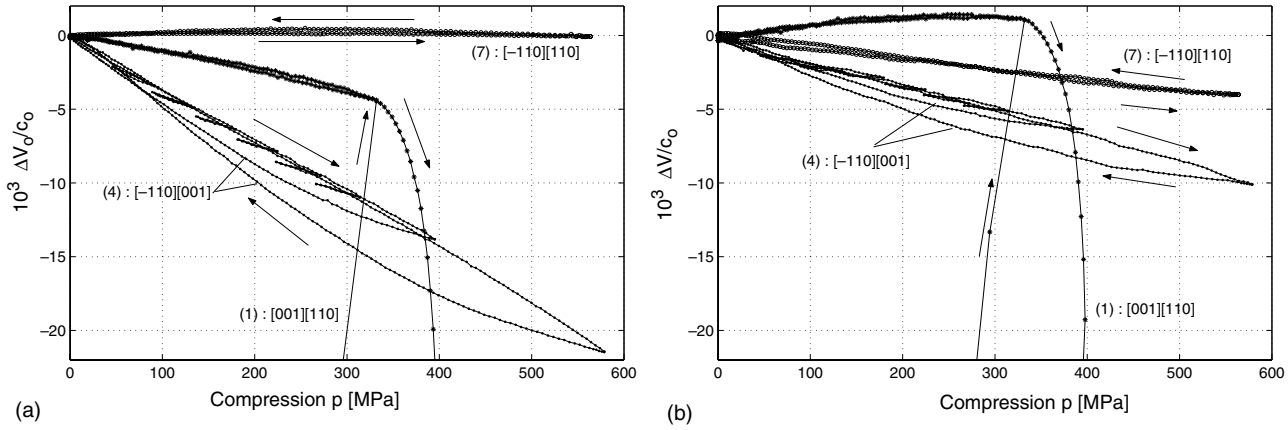

Fig. 7. Velocity changes of all longitudinal modes (mode no.: $[M][N]$) measured by immersion technique with respect to (a) the natural and (b) the deformed state.

strain (stress) however differs significantly among the signals. The AE signal starts to grow at first ($p = 300$ MPa), than the wave speed and attenuation changes due to MT related events are triggered (still in the apparently elastic range) and finally, the transversal strain and macroscopic stress, p evidence the onset of macroscopic transformation process. The reason for these differences comes from the fact that different signals are sensitive to different changes in material state associated with MT. While the acoustic emission is generated by a local and dynamic changes, the wave speed and attenuation characterize average quantity over the specimen, the macroscopic stress and transverse strain relate to the volume fraction of the transformed phase.

Finally, let us return back to the multiple acoustoelastic modes in which the TOECs were measured. The wave speed changes measured in all longitudinal modes during the loading up to 600 MPa are compared in Fig. 7a and b. By loading in the [1 1 0] or [$\bar{1}$ 1 0] directions the loading level 600 MPa is not sufficient to initiate the MT at room temperature due to the orientation dependence of transformation stress. The MT starts above $p = 800$ MPa compression stress together with an irreversible deformation (plasticity). Removing the elastic deformation influence on the wave speed change have an opposite effect on the signal measured in mode #(7) and in modes #(1) and #(4) (compare Fig. 7a and b). This is caused by the negative Poisson's ratio $\nu_{1'2'} = \nu_{2'1'} = -0.62$ corresponding to the modes #(1) and #(4).

The peculiar mode #(4) with hysteresis (Fig. 3a) was measured with partial unloadings to test whether the hysteresis is present (Fig. 7). Taking advantage of the simultaneously measured transverse strain, the changes of instantaneous velocity $\Delta v/c_0$ may be evaluated due to subtraction of the transverse deformation. Since the hysteresis is present even for unloading at smallest stresses, it is not related directly to the MT. Contrary to the mode #(4), the mode #(7) does not show the hysteresis effect. No explanation is available yet but dissipative mechanisms based on the diffusion processes in the crystal are possible candidates.

6. Conclusions

Behavior of the Cu–Al–Ni single crystal ahead of, during, and at the end of the martensite transformation were characterized by ultrasonic pulse-echo methods. Second order elastic constant of the cubic austenite phase were evaluated. The acoustoelastic effect in austenite state was investigated in compression tests at room temperature. Due to the high anisotropy of the parent phase, the measured velocity changes due to the applied stress were found to be strongly dependent on the used configuration of uniaxial compression axis and wave propagation directions in the crystal. The initial slopes of the stress dependencies of natural wave velocities were measured in nine different geometrical configurations and utilized for determination of third order elastic constants of the cubic austenite.

A two wave path immersion technique was adopted for simultaneous measurement of instantaneous thickness and wave velocity in the pseudoelastically deformed Cu–Al–Ni single crystal in compression. The results obtained in the compression test along the [0 0 1] crystal axis using longitudinal wave mode are presented and compared with the results of additional measurements of attenuation and acoustic emission in the same geometrical configuration. The individual acoustic quantities detect the stress-induced martensitic transformation earlier (in the order AE, wave velocity, attenuation) than it can be recognized from the stress–strain record.

Acknowledgements

This work has been supported by Czech Grant Agency under the Post-doc. project no. 106/00/D106 and the institutional project AV CR no. AVOZ2076919.

References

[1] M.A. Breazeale, J. Philip, Determination of third-order elastic constants from ultrasonic harmonic generation measurements, in: W.P. Mason, R.N. Thurtson (Eds.), Physical Acoustics, vol. XVII, Academic Press, London, UK, 1984, pp. 2–61.
[2] A. Gonzàles-Comas, Ll. Mañosa, Philos. Mag. A 80 (2000) 1681–1697.
[3] E.P Papadakis, T.P. Lerch, Pulse superposition, pulse-echo overlap and related techniques, in: M. Levy, H.E. Bass, R.R. Stern (Eds.), Handbook of Elastic Properties of Solids, Liquids and Gases, vol. I–IV, Academic Press, 2001.
[4] D.Y. Li, X.F. Wu, T. Ko, Philos. Mag. A 65 (1991) 585–601.
[5] R.N. Thurston, K. Brugger, Phys. Rev. 133 (1964) A1604–A1610.
[6] D.K. Hsu, M.S. Hughes, J. Acoust. Soc. Am. 92 (Pt.1) (1992) 669–675.
[7] P. Šittner, V. Novák, N. Zárubová, Acta Mater. 46 (1998) 1265–1281.
[8] M. Landa, V. Novák, M. Blaháček, P. Šittner, J. Acoust. Emiss. 20 (2002) 163–171.